



# The Potential of Pulsed Electron Spin Resonance for Tooth-Based Retrospective Biodosimetry

Lotem Buchbinder, et al. [full author details at the end of the article]

Received: 2 May 2021 / Revised: 28 July 2021 / Accepted: 10 August 2021 /  
Published online: 23 August 2021

© The Author(s), under exclusive licence to Springer-Verlag GmbH Austria, part of Springer Nature 2021

## Abstract

Large-scale triage after major radiological events, such as nuclear reactor accidents, requires a method of ionizing radiation dose estimation called retrospective biodosimetry (RBD) to detect doses in the range of 0.5–8 Gy. A well-known technique for performing RBD is electron spin resonance (ESR), which can be used to measure radiation-induced paramagnetic defects in the enamel of the teeth. The concentration of these defects is linearly correlated with radiation doses in the applicable range. Despite its great potential and proven results when applied to extracted teeth, ESR still struggles to provide accurate *in vivo* readings. This is mainly because all available ESR-based RBD methods rely on quantitative signals for calculating the concentration of paramagnetic defects in tooth enamel to evaluate the dose. This requires an accurate knowledge of the volume of the measured enamel, which is very difficult to achieve in live subjects (since teeth also include dentin and possibly cavities). Here, we examine radiation-induced paramagnetic defects in the enamel layer of human teeth using advanced pulsed ESR methods, with the ultimate goal of supporting the development of an innovative practical RBD device for *in vivo* use. We employ a variety of pulsed ESR techniques, such as ESR measurements of spin–spin relaxation time ( $T_2$ ), ESR monitoring of instantaneous diffusion decay time ( $T_{ID}$ ), and dipolar ESR spectroscopy, to explore their possible use to quantify the irradiation dose. Moreover, we develop a special resonator for teeth measurements that make use of such pulse techniques to overcome the constraints of small signal magnitudes and short coherence times. Our results show a good correlation between measured values of  $T_2$ ,  $T_{ID}$ , and the irradiated dose, but further work is required to improve the robustness, accuracy, and sensitivity of the methods presented before they could possibly be applied for *in vivo* measurements in typical doses of ~2–8 Gy. These findings and approaches may be used in the future for the development of a RBD device to evaluate ionizing radiation doses without prior knowledge of the measured enamel volume.

## 1 Introduction

Ionizing radiation is a general term for radiation that travels in the form of particles or electromagnetic waves and carries sufficient energy to detach electrons from atoms or molecules, thereby ionizing them. Small-scale exposure to ionizing radiation is fairly common in modern life. It can result, for example, from radioactive materials in the crust of the Earth (such as uranium, thorium, or radon) or cosmic radiation from space, as well as from human-made radiation such as that produced by X-ray or nuclear medicine procedures. Large-scale exposure to ionizing radiation can result from several scenarios, including radiation accidents (such as the 1987 event in Goiânia, Brazil); nuclear reactor accidents (e.g., the 1986 Chernobyl and 2011 Fukushima-Daiichi accidents); and terrorist attacks using radiological dispersal devices. Following any such event, estimation of the dose received by first responders and members of the public who were exposed is critical. The received dose serves as a guideline for mass-casualty triage and helps determine the proper medical treatment. In most scenarios, it would be valuable to differentiate between doses that cause acute radiation syndrome—normally above 2 Gray (denoted as Gy), with 1 Gy representing the absorption of 1 J of radiation energy per kilogram of mass—and doses below that level, which are tolerable [1–3].

The field of medical physics research concerned with measuring the radiation dose absorbed by an individual using biological materials is called biodosimetry [4]. Its main challenge is to provide an effective method for retrospective biodosimetry (RBD) that can be used to solve the problem of triage in mass-casualty events like those described above. In these incidents, few people, if any, wear standard dosimeters such as thermoluminescent or electronic personal devices, and thus it is necessary to conduct a retrospective estimation of the received radiation dose.

Most approaches to RBD are complex and expensive, require a long time for sample preparation and measurement, involve an invasive procedure, and are usually performed far from the scene. This hinders the rapid assessment and effective treatment of exposed individuals in the critical early stages of responding to mass-casualty events. Moreover, biologically based methods are inherently impacted by differences among individuals in their responses to damaging events, and the biological responses necessarily vary over time [5]. Thus, there is a major need to develop a physical RBD method that is fast, inexpensive, reliable, noninvasive, and portable. *In vivo* electron spin resonance (ESR) is considered to be one of the most applicable techniques suited to these types of events [6–8]. ESR measures radiation-induced paramagnetic defects in tooth enamel, the concentration of which is known to proceed linearly with the received radiation dose, ranging from 50 mGy [9] up to hundreds of Gy [10], and to reach saturation at about 100 kGy [11]. It is perhaps the only physical method that can differentiate among doses with sufficient sensitivity and resolution to classify individuals into categories for treatment, and with sufficient accuracy to facilitate decision-making regarding medical treatment [12, 13]. Despite its great potential and proven results when measuring extracted teeth, ESR still struggles to provide sufficiently accurate readings *in vivo*. This is mainly because all available ESR-based methods rely on quantitative continuous wave

(CW) ESR signal measurements of the teeth to obtain the concentration of paramagnetic defects and hence determine the dose received [14–16]. However, such quantitative measurements have inherent limitations for in vivo studies. It is very difficult to know a priori the volume of the measured enamel (since teeth also include dentin and possibly cavities), and thus the measured ESR signal amplitude cannot be accurately correlated with the concentration of paramagnetic defects. Moreover, the signal's amplitude can vary significantly due to many instrumental factors, and as such, it is generally too unreliable to serve as the sole basis for quantifying the measured sample.

Here, we aim to develop new ESR approaches to the evaluation of radiation doses using retrospective biodosimetry. Unlike existing methods, which rely solely on quantitative measurements of the ESR signal's magnitude in an attempt to obtain the defects' concentration, we target other specific unique characteristics such as spin–spin relaxation times and spin–spin dipolar interactions at the nanoscale level. We hypothesize that this type of information, which does not depend on the ESR signal's magnitude, can be directly correlated with the paramagnetic defects' concentration and thus leads straight to the applied radiation dose. This may make it possible to substantially improve the validity and accuracy of practical ESR-based techniques and approaches to tooth-enamel-based retrospective biodosimetry. Previous pulsed ESR measurements and data on irradiated teeth is scarce and focuses mainly on relaxation time ( $T_1$  and  $T_2$ ) measurements [17–20]. These experiments do not include the use of more advanced methods, such as dipolar spectroscopy [21] or looking into the effects of instantaneous diffusion [22]. Accordingly, our efforts here are based on the use of pulsed ESR and pulsed dipolar ESR spectroscopy, both designed to operate in conjunction with special tailor-made resonators for optimal targeting of the human tooth. Following this introduction, we provide details of the experimental methods and the results, which are compared with data obtained from conventional CW ESR. Conclusions are drawn with respect to the prospects of the pulsed-based methodologies for practical in vivo ESR applications.

## 2 Materials and Methods

### 2.1 Samples

#### 2.1.1 Reference Samples

Reference samples of H@POSS and  $\gamma$ -irradiated quartz, with well-known ESR spectra and well-defined spin concentrations, were used in this study to calibrate the number of spins in our teeth samples. This allowed evaluating the ESR system's capabilities and the applicability of the pulse techniques we employed.

- a. H@POSS: Encapsulated atomic hydrogen in polyhedral octa-silsesquioxane (POSS) cages, also known as H@POSS [23, 24], was used as reference sample for the quantitative ESR spin count. It is known that H@POSS is characterized

by a large hyperfine coupling between the electron and the nuclear spin of the hydrogen. This splitting eliminates the overlap between the reference sample and the tooth enamel in the CW ESR spectrum. This fact, combined with its stability at room temperature, makes H@POSS an excellent quantitative reference sample for this work. H@POSS was produced from POSS sealed in a glass tube in an oxygen-rich environment. The sample was irradiated to 300 kGy using a  $^{60}\text{Co}$  gamma source (1.12 MeV) at the Soreq Nuclear Research Center (SNRC) in Yavne, Israel. The number of spins was measured to be  $(3.61 \times 10^{13} \pm 9.01 \times 10^{11} \text{ spins/sample})$  by comparing it to the CW ESR signal of a solution of a stable organic radical with known concentration.

- b.  $\gamma$ -irradiated quartz: Irradiated quartz is a good model system for many types of stable paramagnetic defects in irradiated solids. It has well-characterized E' paramagnetic centers that have long relaxation times at room temperature, a strong signal, and high stability [25–27]. Irradiated quartz samples were prepared using the following procedure: The raw material samples in the form of quartz rods (2 cm long and 2.9 mm in diameter, with a density of  $2.65 \text{ g/cm}^3$ ) were irradiated using a  $^{60}\text{Co}$  gamma source and given different doses: 1, 10, and 100 kGy. The samples were processed at the irradiator of the Bio-Fly company (Sde Eliyahu, Israel). Subsequently, the pieces were ground up and then sealed in a capillary tube. CW ESR measurements were carried out to evaluate the spin concentration of the quartz samples, which was determined by comparing the double integral CW ESR signal to that of a solution of a stable organic radical with known concentration. The results are summarized in Table 1, which shows the error evaluated from the standard deviation divided by the average of five measurements. Our data are also compared to the spin concentration found in irradiated natural quartz as described in the literature [25].

## 2.1.2 Teeth Samples

Several dozens of incisor teeth were purchased from the Science Care Company (USA) and were used with approval from the Technion's Ethics Committee (Fig. 1a). Tooth portions were irradiated at the SNRC's Secondary Standard Dosimetry Laboratory using a  $^{137}\text{Cs}$  gamma source ( $\sim 0.66 \text{ MeV}$ ), at several doses: 1, 5, 10, 50, 100,

**Table 1** Spin concentration of E' paramagnetic defects in irradiated quartz

Dose [kGy]	Spin concentration [Spin/cm <sup>3</sup> ]	Error [Spins/cm <sup>3</sup> ]	Error [%]	Spin concentration [25] [Spins/cm <sup>3</sup> ]
1	$2.29 \times 10^{16}$	$1.98 \times 10^{15}$	8.64	$2.15 \times 10^{16}$
10	$5.78 \times 10^{16}$	$1.02 \times 10^{16}$	17.65	$5 \times 10^{16}$
100	$12.8 \times 10^{16}$	$2.98 \times 10^{16}$	23.26	$9.4 \times 10^{16}$

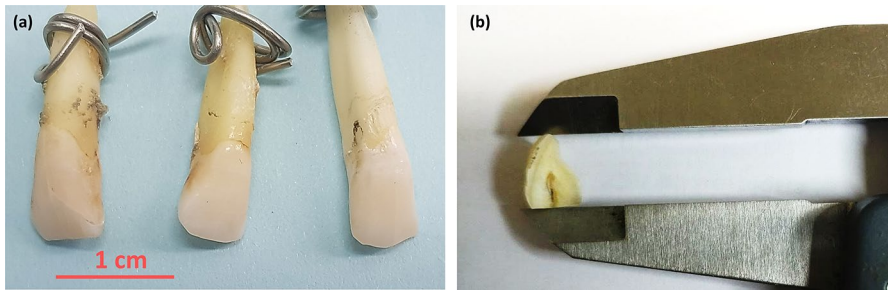


**Fig. 1** **a** Typical intact (uncut) teeth. **b** Typical tooth profile after the cut and before chemical etching

500, and 1000 Gy. Other portions were irradiated using a  $^{60}\text{Co}$  gamma source at the SNRC Space and Materials Department at doses of 10, 50, 100, and 500 Gy.

For in vitro measurements, such as those carried out in this work, the common practice for preparing enamel samples involves mechanical and chemical etching [10] that results in the removal of most of the dentin. Accordingly, we cut the teeth's crowns from the roots using a diamond knife (Fig. 1b). The crown was etched using a 30% NaOH solution in an ultrasonic bath at 65 °C for about 3 h. After washing thoroughly with water and drying, the leftover dentin was removed by a dermal drilling tool and the teeth samples were manually crushed into small pieces using hand tools. In some studies (see Appendix 1), we measured the complete teeth as acquired, with no additional treatment (other than the irradiation).

## 2.2 Research Methods

### 2.2.1 Continuous Wave ESR

Continuous wave (CW) ESR measurements were carried out using a commercial X-band ESR spectrometer (Bruker EMX). The measurements were taken at a frequency of  $\sim 9.4$  GHz, with a sweep step of 0.19 G, power = 20.02 mW, modulation frequency = 100 kHz, modulation amplitude = 1 G, conversion time = 40.96 ms, and time constant = 163.84 ms, using 10 scans.

### 2.2.2 Pulsed ESR System

Some of the pulsed ESR measurements were carried out at Q-band frequencies using a Bruker Elexsys E580 outfitted with a Q-band resonator (EN-5107-D2) at the Weizmann Institute of Science. For variable temperature experiments, an Oxford Instruments CF935 continuous flow cryostat was employed to control the temperature using liquid nitrogen. In addition to the Q-band system, some of the measurements were carried out at X-band frequencies using a spinUP-X system by Spinflex Instruments Ltd. The X-band system's advantages included the possibility of measuring intact teeth and the flexibility of its software. This system was composed of an electromagnet to generate a static magnetic field; a microwave reference source

providing an MW signal with well-defined frequency; a microwave bridge to transmit a chosen pulse sequence and receive the signal from the sample; and an arbitrary waveform generator (AWG) that provided greater flexibility in experimental design and operating frequency. The AWG unit allowed for control over the shape and amplitude of the pulses, while the computer used to operate the system controlled the pulse sequence and the main magnetic field and performed signal processing. The X-band pulsed spectrometer also made it possible to work at much higher repetition rates (up to 400 kHz) compared to the Q-band system with its TWT amplifier (which typically reaches only 500–2000 Hz), implying much faster acquisition times for species with a short  $T_1$ , such as the teeth examined here. Therefore, the bottom-line sensitivity for a given acquisition time was found to be similar in both systems. The X-band system was operated in conjunction with a dielectric resonator built especially for the efficient measurement of small tooth samples in this project (see below).

### 2.2.3 Resonator

The X-band resonator constructed for this work makes it possible to deal with the low number of spins expected for most teeth samples and to carry out pulsed experiments with the modest ( $\sim 20$  W) power available in our system. The resonator we employed in this study (called  $D_B$ ) is capable of accommodating samples with fairly large volumes and therefore facilitates a relatively large concentration sensitivity [28], as well as enabling the measurement of intact teeth when needed. It is made of a material with a dielectric constant of 38 and dielectric loss ( $\tan \delta$  of  $\sim 0.0005$  at 10 GHz (machined from part # DRT099V030C044 from Murata), and its dimensions (outer diameter 8.4 mm, inner diameter 6.5 mm, height 2.5 mm) allow it to operate at a frequency of  $\sim 9.4$  GHz. Figure 2 shows the overall design of the resonator and its calculated microwave magnetic field, as well as its  $S_{11}$  plot without and with teeth material in it. The homogeneity of  $B_1$ , as reflected from the data shown in Fig. 2c, is  $\sim 20$ –60%, depending on how far the sample is extended towards the inner walls of the resonator and/or above or below the resonator's ring. Such homogeneity is sufficient for the relaxation measurements ( $T_1$ ,  $T_2$ ) employed here. More complex experiments such as microwave mutations [29], magnetization transfer [30], and spin-counting DEER measurements [31] may require better homogeneity, but these were not employed here. The resonator's  $Q$ -factor is  $\sim 550$  and  $\sim 300$  without and with the teeth material, respectively (Fig. 2d). Its spin sensitivity for the type of stable radicals generated in teeth is  $\sim 10^{12}$  spins for 1 s of averaging time. In terms of concentration sensitivity, we obtained a signal-to-noise-ratio (SNR) of  $\sim 100$  for the 100 Gy tooth (spin concentration of  $\sim 10^{16}$  spins/cm<sup>3</sup>; see below) for 1 s of averaging time, when the resonator was filled with teeth pieces. The design also includes a sample holder as well as field-jump coils that reduce the field-independent ring-down noise of the measurement from the signal and thus improve the measurement dead time. This is achieved by performing two consecutive measurements, one without current in the coil (on-resonance, which gives an ESR signal) and one with current in the coil (off-resonance, which would give only a background and ring-down "signal"), and subtracting the measured signal in the two cases.

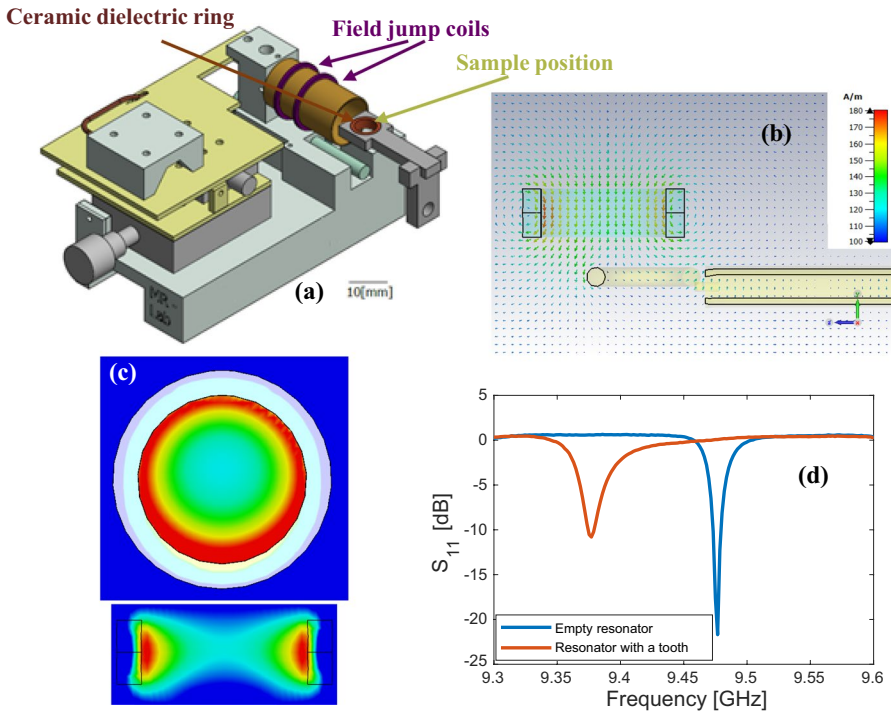


**Fig. 2** The  $D_B$  resonator. **a** The entire assembly. **b** Calculated  $B_1$  fields inside the  $D_B$  resonator, as performed by CST finite-element electromagnetic simulation software. The plot also shows the coupling loop below the resonator. **c** Plots of the microwave magnetic field inside the resonator (two orthogonal cross sections). The magnitude color scale is the same as that shown in **b**. **d** Reflection coefficient ( $S_{11}$ ) measured for the empty resonator (blue) and for the resonator with a tooth in it (red) (Color figure online)

### 2.2.4 Data Analysis

The pulsed ESR echo signal was integrated to obtain its magnitude. Theoretical fits to relaxation curves were obtained using single or bi-exponential functions. In some cases, we also fitted multi-exponential curves to obtain a distribution of relaxation times using UpenWin software [32], where the signal is modeled by a sum of decaying exponential functions with some added noise/bias:

$$s(t_i) = g_0 + \sum_{k=1}^M g_k e^{-t_i/T_k}. \tag{1}$$



### 3 Results and Discussion

#### 3.1 Spin Concentration

The spin concentration of the irradiated teeth samples was evaluated by comparing the double integral of their CW ESR signal at X-band to a reference sample of H@POSS with a known number of spins. We measured teeth irradiated by two types of radiation sources ( $^{137}\text{Cs}$  and  $^{60}\text{Co}$ ) to learn more about their energy response, i.e., the response of a material to different ionizing radiation energies and sources. Specifically, in our case, this refers to the various quantities of defects generated by the same dose of ionizing radiation using different energy sources. In tooth dosimetry research, most irradiation protocols employ a  $^{60}\text{Co}$  source due to its high gamma energy ( $\sim 1.2$  MeV), wide availability, and extensive use in the industrial and medical sectors. Certain studies concerning synthetic hydroxyapatite and tooth enamel found no energy dependence in the response to various sources between 58 and 1250 keV [33, 34], though a difference of up to 8% was identified in energies lower than 50 keV. Other studies, however, have shown a significant dependence of ESR signals on the radiation energy of X-ray beams and of  $^{137}\text{Cs}$  and  $^{60}\text{Co}$  gamma rays [35–39]. For example, Hassan et al. [35] found that the energy response for defect concentrations produced by sources at low energies (less than 100 keV) was five times higher than the response resulting from  $^{60}\text{Co}$ , while that produced by  $^{137}\text{Cs}$  was 20% lower than the one generated by  $^{60}\text{Co}$ . Significant differences in energy response for enamel ESR measurements would limit the latter's effectiveness for dose evaluation and their use as an RBD tool. Here, we took several teeth from one supplier and divided them into two groups, one irradiated using a calibrated  $^{60}\text{Co}$  source and the other using a calibrated  $^{137}\text{Cs}$  source (662 keV), with different doses. We chose a single supplier to reduce any biological diversity that could influence the enamel's energy response.

Table 2 and Fig. 3 show the summary of the spin concentration measurements according to irradiation dose, obtained from three samples for each dose. A good linear correlation between spin concentration and dose was found for both the  $^{137}\text{Cs}$  and  $^{60}\text{Co}$  sources. Figure 3 also provides a comparison to previous literature, in which the absolute spin concentration was estimated using external

**Table 2** Spin concentration in spins/cm<sup>3</sup> for teeth irradiated by  $^{60}\text{Co}$  and  $^{137}\text{Cs}$  sources

Dose [Gy]	Radiation source					
	$^{60}\text{Co}$	SD	Error [%]	$^{137}\text{Cs}$	SD	Error [%]
1000				$7.75 \times 10^{16}$	$2.42 \times 10^{16}$	31
500	$3.87 \times 10^{16}$	$1.32 \times 10^{16}$	34	$5.25 \times 10^{16}$	$7.95 \times 10^{15}$	15
100	$1.09 \times 10^{16}$	$5.30 \times 10^{15}$	48	$1.28 \times 10^{16}$	$6.51 \times 10^{14}$	5
50	$7.25 \times 10^{15}$	$3.14 \times 10^{15}$	43	$4.78 \times 10^{15}$	$5.49 \times 10^{14}$	11

SD is the standard deviation of the measured values; error is the relative error expressed as a percent based on the SD value



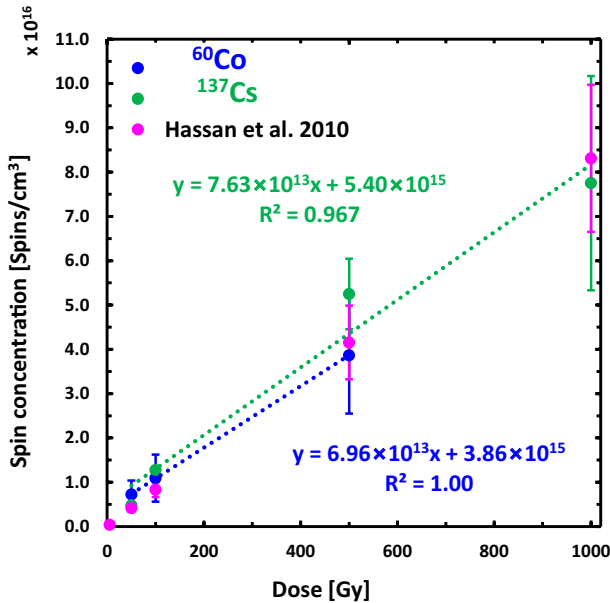


**Fig. 3** Dose–response plot showing spin concentration as a function of dose for irradiated teeth using  $^{137}\text{Cs}$  (green line),  $^{60}\text{Co}$  (blue line), and data from previous literature (magenta dots) (Color figure online)

references and found to have an error of 20% [35]. In that work,  $^{60}\text{Co}$  was used to generate defects and the dose response was found to be  $8.31 \times 10^{13}$  [spins/ $\text{Gy}\cdot\text{cm}^3$ ] [35].

The data we gathered shows that in samples irradiated with  $^{137}\text{Cs}$ , the dose response (the slope of the line) is slightly larger than that of samples irradiated with  $^{60}\text{Co}$  (namely,  $6.96 \times 10^{13}$  and  $7.63 \times 10^{13}$  [spins/ $\text{Gy}\cdot\text{cm}^3$ ] for  $^{60}\text{Co}$  and  $^{137}\text{Cs}$ , respectively). However, this ~9% difference between the two types of sources is within the error range. The slopes we found have slightly lower values than those found in ref [35]. These differences could be attributed to residual dentin from the etching process resulting in a lower calculated spin concentration; to other measurement errors; or to biological diversity, as reflected by the relatively large standard deviation in our results.

### 3.2 $T_1$ and $T_2$ Relaxation Times

The first and simplest type of spectroscopic markers we examined as possible candidates for the quantitative evaluation of spin concentration are the spin–lattice ( $T_1$ ) and spin–spin ( $T_2$ ) relaxation times. Here, we present our results of  $T_1$  and  $T_2$  measurements for a variety of samples at different temperatures and attempt to correlate them with the spin concentration. The data is provided first for the quartz test samples to verify our methodology, and subsequently for the teeth.

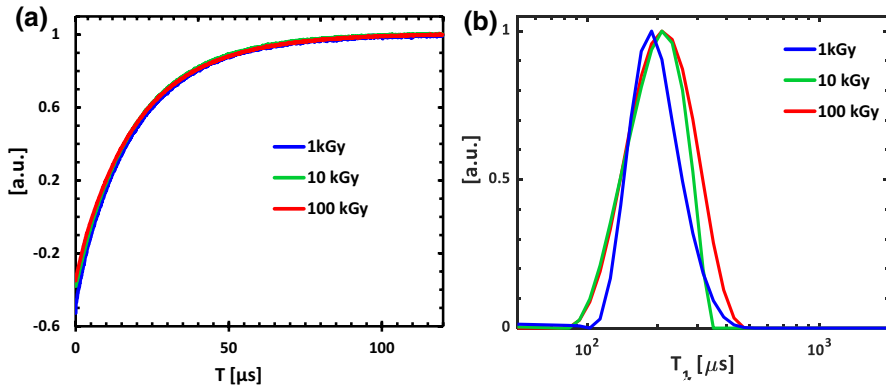


**Fig. 4** **a** Inversion recovery experiment results of  $T_1$  in irradiated quartz samples. Measurements were carried out at  $\sim 33.66$  GHz, with  $\pi/2$  pulse length of 16 ns.  $T$  is the time interval between the inversion pulse to the subsequent Hahn echo sequence. **b** Distributions of  $T_1$  calculated by UpenWin from inversion recovery curves in irradiated quartz samples

**Table 3**  $T_1$  relaxation times in quartz samples obtained using an exponential model and the dominant term in the UpenWin distribution analysis

Dose [kGy]	Exponential fit [ $\mu$ s]	UpenWin distribution's max. value [ $\mu$ s]
100	201.8	209.8
10	194.6	209.8
1	193.1	189.4

### 3.2.1 Spin–Lattice Relaxation, $T_1$

**3.2.1.1 Irradiated Quartz** Spin–lattice relaxation curves measured using inversion recovery pulse sequences at room temperature are shown in Fig. 4a, and the relaxation times are summarized in Table 3. They show no significant or meaningful dose dependence, which is plausible since the lattice is the same for all doses and defects are not formed in sufficiently high concentrations to change the lattice. The  $T_1$  distribution analysis, obtained using UpenWin software (Fig. 4b), indicates that at room temperature, there is primarily one dominant energy exchange mechanism between the spins and the lattice.

**3.2.1.2 Irradiated Teeth** While quartz samples show a fairly simple relaxation picture, the  $T_1$  distribution of irradiated teeth samples reveals a more complex behavior, as shown in Fig. 5. Such complexity also appears in the literature [20], and therefore, we tested also a bi-exponential model to fit the data. The results for the  $^{60}\text{Co}$  irradiated samples are summarized in Table 4 (the data regarding  $^{137}\text{Cs}$  is very similar).

The peak at the short  $T_1$  can be related to  $\text{CO}_2^-$  substituting phosphate in the hydroxyapatite crystal (B-site), and the longer  $T_1$  values are linked to an organic

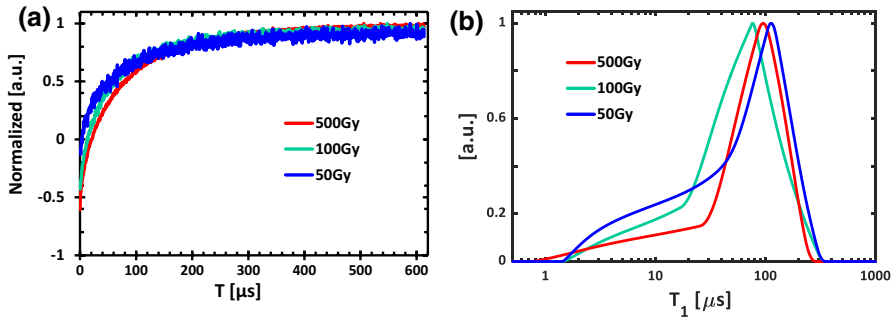


**Fig. 5** **a** Inversion recovery experiment results of  $T_1$  in irradiated teeth samples using a  $^{60}\text{Co}$  source. The experimental parameters are similar to those given in Fig. 4 (Q-band frequency). **b** Distributions of  $T_1$  calculated by UpenWin from inversion recovery curves

**Table 4**  $T_1$  relaxation times in teeth samples, obtained using a bi-exponential decay model and from the dominant term in the UpenWin distribution analysis

Dose [Gy] $^{60}\text{Co}$	Bi-exponential decays [μs]	UpenWin distribution's max. value [μs]
500	173.3	49.0
100	214.0	67.3
50	257.5	88.8

radical inclusion in the teeth [20, 40]. Neither contribution displays a meaningful dose dependence (the same picture occurs also for the  $^{137}\text{Cs}$  source data). Thus, samples irradiated with different doses show no meaningful dose dependence in  $T_1$ , as seen from the data presented in Table 4 and from the UpenWin distribution shown in Fig. 5b.

In conclusion,  $T_1$  shows no significant conclusive dose dependence in both quartz and irradiated tooth enamel, and therefore, cannot be used for dose estimation.

### 3.2.2 Spin-Spin Relaxation ( $T_2$ )

**3.2.2.1 Irradiated Quartz** While  $T_1$  shows no significant dose dependence, such dependency can be easily detected for spin-spin relaxation times ( $T_2$ ) in irradiated quartz samples (Fig. 6a). Specifically, the higher the dose, the faster the echo decay, meaning shorter  $T_2$  values (Table 5). The data can be fitted to a stretched exponential curve, based on the expression:

$$S(\tau) = S_0 \cdot \exp\left(-\frac{2\tau}{T_m}\right)^x, \tag{2}$$

where for  $x=1$ , it represents a simple exponential decay. In addition, the  $T_2$  distributions extracted using UpenWin (Fig. 6b) show distinct differences between samples irradiated with different doses, with  $T_2$  for the maximum value on the distribution varying from 3.8 to 31 μs.

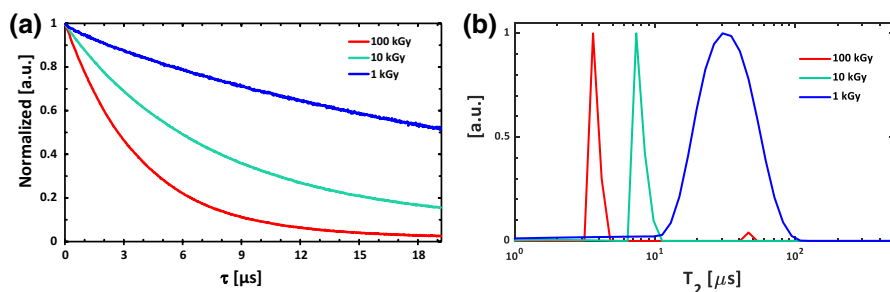


**Fig. 6** **a** Results of echo decay experiments in irradiated quartz at room temperature ( $\sim 34.184$  GHz), normalized intensity versus  $\tau$ . **b** Normalized distributions of  $T_2$  calculated by UpenWin from echo spin decay curves of irradiated quartz at room temperature

**Table 5**  $T_2$  relaxation times in quartz samples obtained by fitting the data to single and stretched exponential decay models and from the UpenWin distribution analysis

Dose [kGy]	Exponential decay		UpenWin distribution's max. value [ $\mu$ s]	Stretched exponential decay parameters		
	$T_2$ [ $\mu$ s]	$R^2$		$x$	$T_2$ [ $\mu$ s]	$R^2$
100	$3.78 \pm 0.003$	1	3.6	0.99	$3.8 \pm 0.001$	1
10	$7.52 \pm 0.002$	1	7.3	0.97	$7.6 \pm 0.011$	1
1	$21.12 \pm 0.05$	1	30.3	0.89	$31.0 \pm 0.01$	1

**3.2.2.2 Irradiated Teeth** Having observed the existence of a strong dose dependence in quartz, we used the same method on irradiated teeth enamel samples. Previous data from the literature revealed a strong dose dependence for  $T_2$ , but only when measured at low temperatures [20]. In our experiments, carried out at room temperature, it was harder to detect a dose dependency from the decay curves themselves (Fig. 7a, c), especially when compared to quartz. Nevertheless, further analysis did reveal some considerable differences. For example, the fitting to a mono-exponential decay function and the analysis of the UpenWin distributions (Figs. 7b, d) showed a meaningful spread and dose-dependent variations, even at room temperature. These results, as well those measured at temperatures of 140 and 85 K, are summarized in Table 6. It is evident that the dose dependence can be inferred not only from the dominant decay time, but also from the distribution shape—high doses produce narrower distributions. The distribution shape suggests the existence of at least two components of the relaxation mechanism, resulting in a wide range of relaxation times. The analysis of the decay curves can also be performed by fitting the data to a stretched exponential decay function, as provided in Table 7. Here also, the same trend of lower doses corresponding to longer relaxation times is evident. An additional insight is that the stretch parameter,  $x$ , increases as temperature is reduced, which implies that other mechanisms are being “shut down”. This leaves us only with one dominated decay mechanism for  $T_2$  at low temperatures.

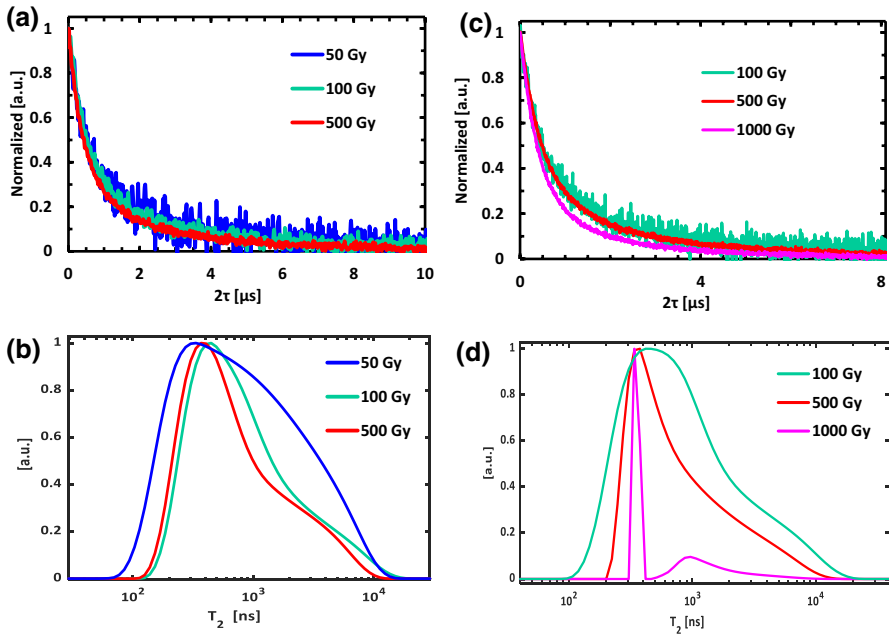


**Fig. 7** **a**  $T_2$  echo spin decay curves in teeth irradiated with  $^{60}\text{Co}$  to 50, 100, and 500 Gy (at  $\sim 34.126$  GHz), measured at room temperature, normalized intensity versus Hahn echo interpulse distance,  $\tau$ . **b** Distributions of  $T_2$  calculated using UpenWin from echo spin decay curves shown in plate (a). **c**  $T_2$  echo spin decay curves in teeth irradiated with  $^{137}\text{Cs}$  to 100, 500, and 1000 Gy (at  $\sim 34.126$  GHz), measured at room temperature, normalized intensity versus interpulse distance,  $\tau$ . **d** Distributions of  $T_2$  calculated using UpenWin from echo spin decay curves shown in plate (c)

### 3.3 Instantaneous Diffusion

Instantaneous diffusion (ID) is a relaxation mechanism that depends on the average distance between spins and is caused by their flip due to the  $\pi$  refocusing pulse in the echo sequence [22]. This mechanism adds another factor to the relaxation process, so that the overall observed relaxation rate in the Hahn echo sequence is as follows:

$$\frac{1}{T_m} = \frac{1}{T_{ID}} + \frac{1}{T_2}, \tag{3}$$

where  $T_m$  is the memory time of the spin system corresponding to echo signal decreases by a factor of e,  $T_2$  is the “intrinsic” spin–spin relaxation time at the limit of the diminishing second pulse in the Hahn echo sequence, and  $T_{ID}$  is the relaxation time generated by the ID mechanism. We can take advantage of instantaneous diffusion and study  $T_m$  as a function of the amplitude (flip angle) of the second pulse in the echo sequence,  $\theta$ , [41, 42]. It is known that  $T_{ID}$  depends on  $\theta$  (which can go from 0 up to  $\pi$ ) according to the expression [22], sec. 8.1.5:

**Table 6**  $T_2$  relaxation times in tooth samples in nanoseconds, obtained using UpenWin distributions and a single exponential model

Dose [Gy]	Source	UpenWin distribution's max. value						Single exponential decay					
		298 K		140 K		85 K		298 K		140 K		85 K	
		$T_2$	$R^2$	$T_2$	$R^2$	$T_2$	$R^2$	$T_2$	$R^2$	$T_2$	$R^2$	$T_2$	$R^2$
1000	$^{137}\text{Cs}$	339	2445	4123	4123	659.4±1	0.9999	2171±3	0.9999	4035±36	0.998		
500	$^{137}\text{Cs}$	376	2639	4123	4123	865.1±2	0.9999	2648±18	0.9977	4128±5	1		
100	$^{137}\text{Cs}$	418	3012	4286	4286	951.5±4	0.9992	2639±27	0.9943	4341±5	1		
50	$^{137}\text{Cs}$	794	3648	4203	4203	2079±422	0.953	2682±233	0.948	4360±5	1		
500	$^{60}\text{Co}$	368	2496	3503	3503	1014±5	0.9995	2688±4	0.9999	3626±2	1		
100	$^{60}\text{Co}$	447	2347	3887	3887	1030±6	0.9993	2648±18	0.9977	3889±3	1		
50	$^{60}\text{Co}$	334	2602	4368	4368	1125±74	0.8869	3163±40	0.9924	4341±3	1		

**Table 7**  $T_2$  relaxation times in teeth samples in nanoseconds, as well as the stretch parameter,  $x$ , obtained from the stretched exponential model in Eq. (2)

Dose [Gy]	Source	Stretched exponential decay								
		298 K			140 K			85 K		
		$x$	$T_2$	$R^2$	$x$	$T_2$	$R^2$	$x$	$T_2$	$R^2$
1000	$^{137}\text{Cs}$	0.6064	$395 \pm 2$	0.9999	0.78	$1661 \pm 2$	1.00	1.14	$4236 \pm 4$	1
500	$^{137}\text{Cs}$	0.6067	$545 \pm 2$	0.9999	0.78	$2064 \pm 2$	1.00	0.97	$4241 \pm 1$	1
100	$^{137}\text{Cs}$	0.6701	$681 \pm 38$	0.9639	0.82	$2256 \pm 4$	0.9999	1.07	$4443 \pm 5$	1
50	$^{137}\text{Cs}$	– <sup>a</sup>	– <sup>a</sup>	– <sup>a</sup>	– <sup>a</sup>	– <sup>a</sup>	– <sup>a</sup>	1.05	$4730 \pm 4$	0.9999
500	$^{60}\text{Co}$	0.578	$481 \pm 3$	0.9998	0.77	$2043 \pm 2$	1.00	1.06	$3746 \pm 2$	1
100	$^{60}\text{Co}$	0.6407	$638 \pm 8$	0.6407	0.90	$2465 \pm 3$	1.00	1.03	$3933 \pm 3$	1
50	$^{60}\text{Co}$	0.5842	$650 \pm 93$	0.906	0.83	$2866 \pm 44$	0.995	1.02	$4370 \pm 4$	1

<sup>a</sup>Could not be analyzed accurately enough due to low signal-to-noise ratio

$$\frac{1}{T_{ID}(\beta)} = C \frac{\pi}{9\sqrt{3}} \frac{\mu_0 g^2 \beta_e^2}{\hbar} \sin^2\left(\frac{\theta}{2}\right), \tag{4}$$

where  $C$  is the concentration of spins [spin/m<sup>3</sup>],  $g$  is the  $g$ -factor value,  $\beta_e$  is the Bohr magneton, and  $\mu_0$  is the vacuum permeability. This means that if we plot  $1/T_m$  and a function of  $\sin^2\left(\frac{\theta}{2}\right)$ , we get a straight line with a slope of  $C \frac{\pi}{9\sqrt{3}} \frac{\mu_0 g^2 \beta_e^2}{\hbar}$  and intercept of  $1/T_2$ , thereby easily extracting our parameter of interest,  $C$ .

In our measurements at Q-band, the flip angles were modified by changing the excitation power, which caused both the first and second pulses in the echo sequence to be smaller. This is a valid approach in cases where it is not possible to independently change the power of the first and second pulses [42], but it has the disadvantage of losing much of the signal when going to low powers (small flip angles). For measurements at X-band with a system equipped with AWG, we only modified the amplitude of the second pulse and thus improved the sensitivity at low flip angles. In this case, instantaneous diffusion was used for quantitative estimation of the local spin concentration. The latter may be different from the average spin concentration if the spins generated by the irradiation process are not homogeneously distributed throughout the sample.

### 3.3.1 Irradiated Quartz

First, we measured the quartz test samples at room temperature. Typical results for the 10-kGy sample are shown in Fig. 8a, and the full data set for all samples is provided in Fig. 8b and Table 8. In Table 8, we also compare the local concentrations (as measured by the instantons diffusion data) and average spin concentrations (as measured by CW ESR against reference samples), which are found to be similar, as expected from materials in which paramagnetic defects are randomly distributed [22, 42].



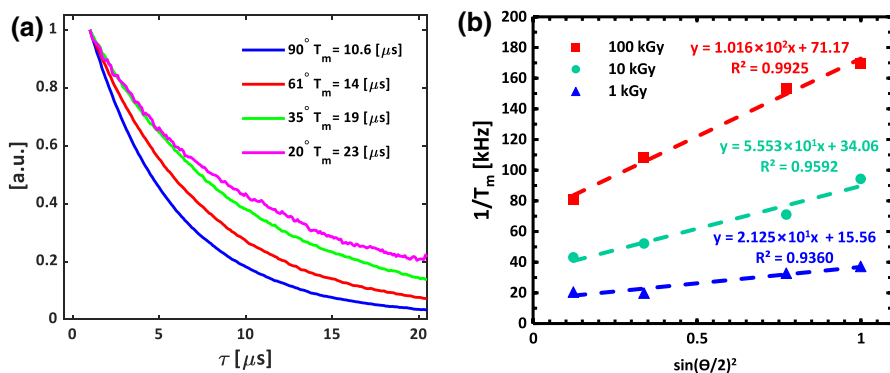


**Fig. 8** **a** Normalized Hahn echo signal intensity versus  $\tau$  for quartz irradiated to 10 kGy, with the corresponding phase memory time ( $T_m$ ) while increasing the flip angle of the first pulse,  $\theta/2$ , from  $20^\circ$  to  $90^\circ$  (with the second pulse flip angle being equal to  $\theta$ ). The measurements were carried out at room temperature and at a frequency of  $\sim 9.58$  GHz. **b** Plot of the reciprocal of the phase memory time ( $T_m$ ) for three types of irradiated quartz samples as a function of the square of the sine of the turning angle of the first pulse ( $\theta/2$ ), measured at room temperature and at  $\sim 9.58$  GHz

**Table 8** Spin concentrations obtained using CW ESR, compared to local concentrations obtained from instantaneous diffusion measurements for irradiated quartz samples measured at room temperature at X-band

Dose [kGy]	Concentration from CW [spins/cm <sup>3</sup> ]	Concentration from ID [spins/cm <sup>3</sup> ]	Intrinsic $T_2$ [ $\mu\text{s}$ ]	$T_m^{\text{min}}$ [ $\mu\text{s}$ ]	Calc $T_{\text{ID}}$ [ns]
100	$12.8 \times 10^{16}$	$12.3 \times 10^{16}$	14.05	5.90	9.44
10	$5.78 \times 10^{16}$	$6.71 \times 10^{16}$	29.36	10.61	20.90
1	$2.29 \times 10^{16}$	$2.57 \times 10^{16}$	64.27	27.00	52.75

We also list the “Intrinsic”  $T_2$  and compare it to  $T_m^{\text{min}}$ , which is the measured memory time for nominal  $90^\circ$  and  $180^\circ$  pulses. The calculated  $T_{\text{ID}}$  is based on Eq. (4), and is obtained using the measured CW-based spin concentrations and assuming  $\theta/2 = 90^\circ$

### 3.3.2 Irradiated Teeth

In contrast to quartz, teeth display a much lower signal to begin with and also suffer from faster signal decay. Accordingly, we first tried to measure instantaneous diffusion at Q-band and at low temperatures to lengthen the relaxation time and enable us to observe the power effects on  $T_m$ . Figure 9a shows the typical dependence of  $T_m$  on the flip angle in tooth enamel samples irradiated with  $^{137}\text{Cs}$  and measured at 140 K, while Fig. 9c presents typical results at 85 K. An analysis using Eq. (3) produced a straight line for both temperatures (Fig. 9b, d). The decrease in signal due to the change in power for both pulses in the sequence limited the lower end of the flip angle that we were able to measure.

The data from teeth measurements is summarized in Table 9. It shows considerable differences between the instantaneous diffusion times for different spin

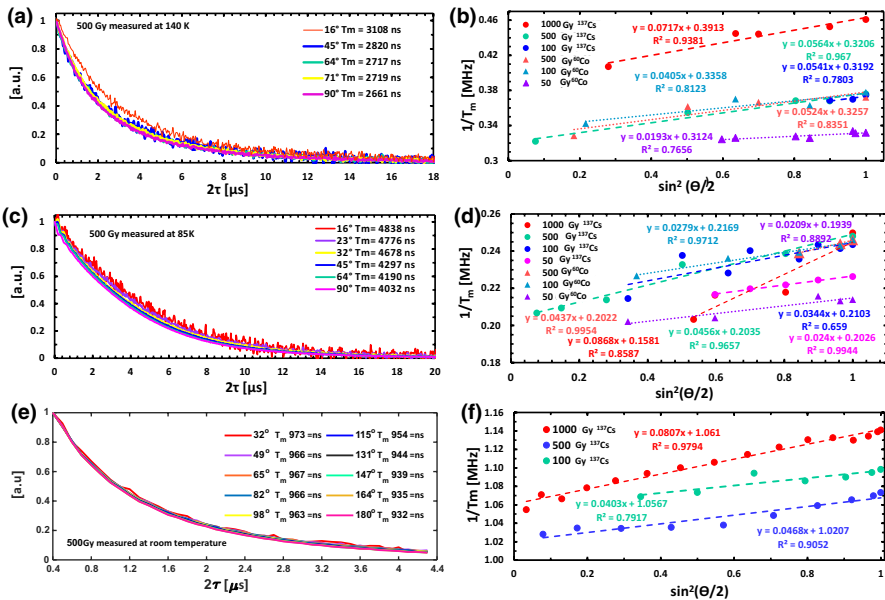


**Fig. 9** **a** Normalized Hahn echo signal intensity versus  $\tau$  for enamel samples irradiated by a  $^{137}\text{Cs}$  source to 500 Gy, with the corresponding phase memory time ( $T_m$ ) as the flip angle of the first pulse is increased from 16° to 90°, measured at 140 K and ~34.27 GHz. **b** Plot of the reciprocal of the phase memory time ( $T_m$ ) for several enamel samples irradiated by different sources and with various doses. As noted in the legend, when measured at 140 K at Q-band, the plot is shown as a function of  $\sin^2\left(\frac{\theta}{2}\right)$ . The slope is a function of the spin concentration. **c** The same as **a** but for measurements at 85 K. **d** The same as **b** for measurements at 85 K. **e** Normalized echo intensity versus  $\tau$  for enamel samples irradiated by a  $^{137}\text{Cs}$  source to 500 Gy, with the corresponding phase memory time ( $T_m$ ) as the flip angle of the second pulse is increased from 32° to 180°, measured at room temperature at X-band. **f** Plot of the reciprocal of the phase memory time ( $T_m$ ) for enamel samples irradiated with  $^{137}\text{Cs}$  to 100, 500, and 1000 Gy, measured at room temperature at X-band, as a function of  $\sin^2\left(\frac{\theta}{2}\right)$

concentrations (different doses). These findings suggest that it would be easy to differentiate between the doses if we could measure the instantaneous diffusion component of relaxation time separately. We see that at low temperatures, the intrinsic  $T_2$  becomes comparable to  $T_{ID}$ , allowing us to easily measure the difference between samples irradiated to different doses. Moreover, even at room temperature, where the contribution of  $T_{ID}$  to  $T_m$  is very small (since the intrinsic  $T_2$  is 1 order of magnitude less than  $T_{ID}$ ), we can still see meaningful trends. This is thanks to the use of the AWG system which allows us to obtain  $T_m$  fits with high accuracy and good sensitivity. Another important observation is that the local concentrations measured by instantaneous diffusion are found to be higher than the average concentrations measured with CW ESR, hinting to the possibility of a nonuniform distribution of the spins. The differences between the local and average concentrations in irradiated teeth are much higher than those found in the quartz samples. This phenomenon is well known in materials irradiated with high LET (linear energy transfer) radiation such as alpha and beta [43]. In

**Table 9** Spin concentration obtained by CW ESR (using H@POSS as a reference sample), compared with local concentration from instantaneous diffusion measured in irradiated teeth samples, based on Q-band measurements at 140 K and 85 K. We also list the “Intrinsic”  $T_2$  and compare it to  $T_m^{\min}$ , which is the measured memory time for nominal  $90^\circ$  and  $180^\circ$  pulses

Source	Dose [Gy]	Temp. [K]	Concentration from CW [spins/cm <sup>3</sup> ]	Concentration from ID [spins/cm <sup>3</sup> ]	Intrinsic $T_2$ [ns]	$T_m^{\min}$ [ns]	Calc $T_{ID}$ [ns]
<sup>137</sup> Cs	1000	140	$7.75 \times 10^{16}$	$8.66 \times 10^{16}$	2171	2555.5	15,587
	500		$5.25 \times 10^{16}$	$7.06 \times 10^{16}$	2661	3137.6	23,009
	100		$1.28 \times 10^{16}$	$6.54 \times 10^{16}$	2714	3133.0	94,375
<sup>60</sup> Co	500	140	$3.87 \times 10^{16}$	$6.33 \times 10^{16}$	2688	3070.1	31,214
	100		$1.09 \times 10^{16}$	$4.89 \times 10^{16}$	2648	2978.0	110,826
	50		$7.25 \times 10^{15}$	$2.29 \times 10^{16}$	3016	3207.2	166,620
<sup>137</sup> Cs	1000	85	$7.75 \times 10^{16}$	$1.05 \times 10^{17}$	4003	4364.9	15,587
	500		$5.25 \times 10^{16}$	$5.51 \times 10^{16}$	4031.8	4914.0	23,009
	100		$1.28 \times 10^{16}$	$4.15 \times 10^{16}$	4106.3	4755.1	94,375
	50		$4.78 \times 10^{15}$	$2.90 \times 10^{16}$	4418.5	4935.8	252,719
<sup>60</sup> Co	500	85	$3.87 \times 10^{16}$	$5.28 \times 10^{16}$	3874.3	4207.0	31,214
	100		$1.09 \times 10^{16}$	$3.4 \times 10^{16}$	4054.4	4610.4	110,826
	50		$7.25 \times 10^{15}$	$2.5 \times 10^{16}$	4675.3	5157.3	166,620
<sup>137</sup> Cs	1000	Room temperature	$7.75 \times 10^{16}$	$9.7 \times 10^{17}$	876.4	942.5	15,587
	500		$5.25 \times 10^{16}$	$5.7 \times 10^{17}$	931.7	979.7	23,009
	100		$1.28 \times 10^{16}$	$4.9 \times 10^{17}$	910.5	946.3	94,375

The calculated  $T_{ID}$  is based on Eq. (4) using the measured CW-based spin concentrations and assuming  $\theta/2=90^\circ$ . The room temperature data is measured at X-band using a system with AWG so that only the second pulse in the Hahn echo sequence is modified

low LET radiation, such as gamma, the distribution of the spins has been found to be uniform only in doses higher than  $\sim 5$  kGy [42], as seen in the quartz samples. The results of our experiments show that the difference between local and average concentrations is reduced when we measure samples irradiated to higher doses (all of our doses were lower than 5 kGy). This suggests that said differences reflects the track effect and not the enamel structure, as suggested by Brik et al. [44] and others, meaning that the track effect is visible in lower doses. Many of the concentrations measured at 140 K are higher than those obtained made at 85 K. However, the 85 K data are more reliable and fits to a single exponential model better than the 140 K data (Tables 6 and 7).

### 3.4 Double Electron–Electron Resonance (DEER)

DEER can be used to directly measure spin dipolar interaction. The DEER background decay of radicals distributed randomly in space follows the expression given by [45]

$$V(t, C) = \exp\left(-\frac{2\pi g^2 \mu_B^2 \mu_0 N_A}{9\sqrt{3}\hbar} \lambda C t\right), \tag{5}$$

where  $g$ ,  $\mu_B$ , and  $\mu_0$  are as described above,  $N_A$  is Avogadro’s number, and  $\lambda$  is the fraction of the spins excited by the DEER pump pulse (ranging from 0 to 1). Here, we employ a simple 3-pulse DEER sequence to minimize spin relaxation due to the short  $T_2$  of the teeth samples [46].

### 3.4.1 Quartz Samples

Figure 10 shows the results of the 3-pulse DEER experiment conducted at room temperature at Q-band for the irradiated quartz samples. The data are compared to the theoretical decay via Eq. (5) assuming  $\lambda=0.59$  and using the CW-derived spin concentration values provided in Table 1. These results clearly show that higher doses lead to faster decay. For samples at 10 kGy and 100 kGy, the decay is stronger than was theoretically expected, which can be due to errors in the assessment of  $\lambda$  in different experiments. Overall, it is evident that for quartz samples DEER can provide good information about spin concentration.

### 3.4.2 Teeth Samples

Teeth samples were measured using the same 3-pulse DEER method. The data are provided in Fig. 11. Due to the wide spectrum of the irradiated teeth (Fig. 11a’s inset), it was easier to define a pump pulse that did not overlap with the observer pulse. However, because of the relatively fast relaxation times of the ESR signal

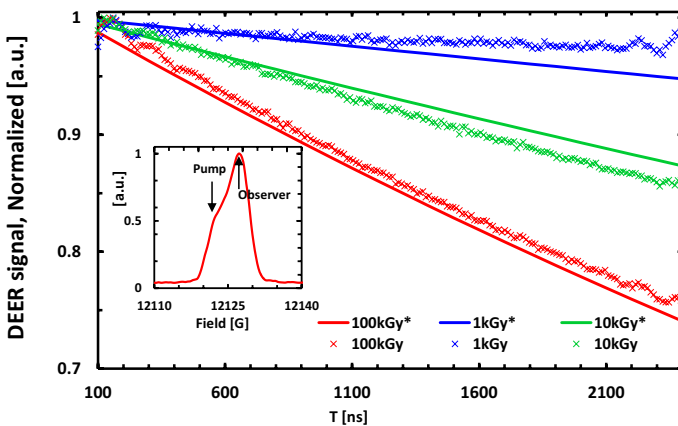


**Fig. 10** Three-pulse DEER signal decay in quartz samples irradiated with different doses (crosses), superimposed by the decay simulation (solid line) with  $\lambda=0.59$ , where T is the time of the pump pulse after the first pulse in the sequence. Typical experimental parameters: frequency = ~33.6 GHz,  $\pi/2$  pulse length = 18 ns, pump pulse length = 32 ns, pump offset frequency = 25 MHz (see inset showing the field-swept echo signal of the samples)

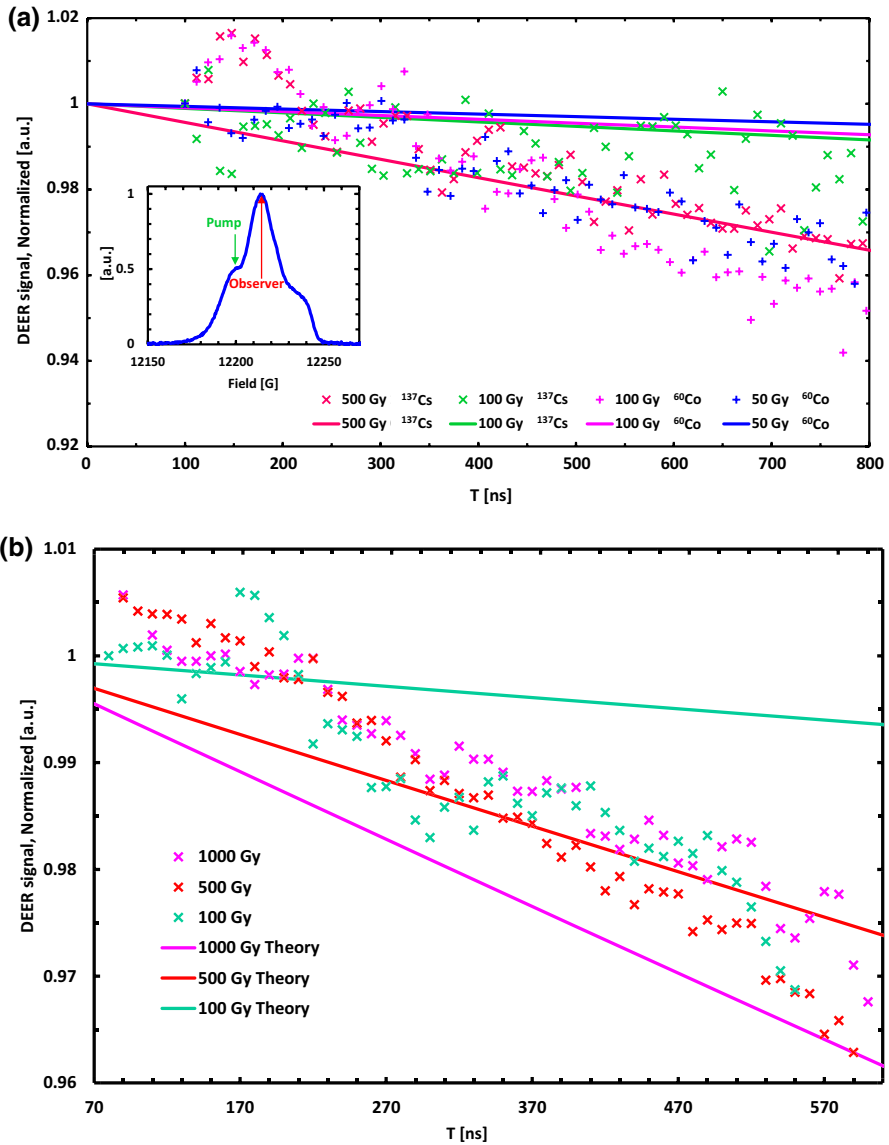


**Fig. 11** **a** Three-pulse DEER signal decay of tooth enamel samples irradiated to various doses with  $^{137}\text{Cs}$  and  $^{60}\text{Co}$ , superimposed by the decay simulation (solid line) with  $\lambda=0.5$ , where T is the time of the pump pulse after the first pulse in the sequence. Typical experimental parameters: Q-band frequency,  $\pi/2$  pulse length = 14 ns, pump pulse length = 28 ns, pump offset frequency = 40 MHz. **b** Three-pulse DEER signal decay in tooth enamel samples irradiated to different doses with  $^{137}\text{Cs}$ , superimposed by the decay simulation (continuous lines) with  $\lambda=0.5$ , where T is the start time for the pump pulse. Typical experimental parameters: X-band frequency = 10.8 GHz,  $\pi/2$  pulse length = 120 ns, pump pulse length = 120 ns, pump offset frequency = 16 MHz

in teeth, the signal decayed quickly and this limited the measurement time. Nevertheless, even though the signal was weak and decayed fast, we were able to measure and record the DEER decay at room temperature both at Q-band and at X-band. Despite the distinct observation of the decay signal, we could not see a clear correlation between the decay rate and the irradiation dose. This, again, may hint to the possibility that the local spin concentration along the irradiation tracks is more or less constant. An additional issue that may interfere with the quantitative measurement of global spin concentrations using DEER is the possible variation in  $\lambda$ , which can affect the accuracy of the measurement.

## 4 Discussion and Conclusions

In this work, we examined the possibility of using advanced pulsed ESR techniques to evaluate the concentration of paramagnetic defects in  $\gamma$ -irradiated teeth samples without having to measure the volume of the enamel in those samples. The ultimate aim of this approach is to facilitate accurate *in vivo* measurements of teeth to estimate the ionizing radiation dose to which a person was exposed, based on the concentration of the paramagnetic defects in his/her teeth. The results we obtained using  $\gamma$ -irradiated quartz samples clearly show that  $T_2$ ,  $T_{ID}$ , and DEER data can be easily correlated with the irradiation dose. Similar measurements in  $\gamma$ -irradiated teeth, based on the same protocols, result in data sets that are harder to correlate with irradiation doses, especially when we limit ourselves to room temperature conditions (which are to be expected when conducting *in vivo* tests). Nevertheless, based on our experiments, we are still hopeful for the potential prospects of using  $T_2$  and especially  $T_{ID}$  measurements to obtain good estimates of irradiation doses in teeth. This, however, would require completing a much larger set of experiments with a variety of teeth, and also clarifying better the issue of the track effect that can be problematic in dose estimation, especially for low doses that are more typical of real-life scenarios. Another issue of concern is the limited sensitivity of pulsed ESR that can be a showstopper regarding the measurement of low doses in the  $\sim 0.5$ – $1$  Gy range. Nevertheless, as we have already shown in the past [12], this aspect can be dealt with using configurations optimized for *in vivo* measurements that can cope rather well with doses of at least 2 Gy. An additional aspect we would like to emphasize is that while our measurements were carried out with teeth subjected to a well-established and common treatment of cleaning and crushing (Sect. 2.1.2), their results are clearly representative of what we can expect from whole intact teeth (see Appendix 1). In conclusion, the present work constitutes a first step towards the possible implementation of pulsed ESR in the *in vivo* retrospective biodosimetry of teeth, but much work is still required to hopefully transform it into a viable approach in the future. In that respect, one possible practice would be to combine the pulsed *in vivo* quantitative measurements of the tip of the tooth [12] with the pulsed spectroscopic measurements of  $T_2$  and  $T_{ID}$ , carried out in this work to provide a more complete and accurate picture.

## Appendix 1: Comparison of ESR Spectroscopic Properties for Intact and Processed Teeth

The teeth examined in this work underwent pre-treatment of chemical and mechanical nature, as described in Sect. 2.1.2. While this procedure that we carried out is well established and appears in many official protocols of ESR dosimetry, it is important to verify that such treatment does not affect the spectroscopic properties we examined here. To answer this question, we compared teeth irradiated by 100, 500, and 1000 Gy, using a  $^{137}\text{Cs}$  source, before and after the pre-treatment procedure. The results of such comparison, carried out for CW spectra, as well as for Hahn echo and inversion recovery measurements, are shown in Figs. 12, 13, 14 for the 500 Gy tooth. The CW spectrum shows slight differences in shape, but for the pulsed data, which is the essence of this work, there are no measurable differences between the results before/after the treatment procedure. The 1000 and 100 Gy (not shown) exhibit the same behavior.

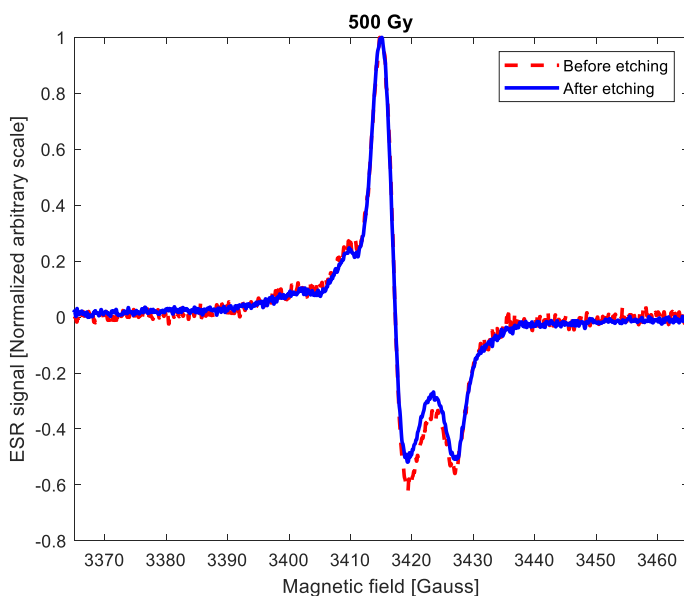


**Fig. 12** Continuous wave ESR spectrum of intact teeth irradiated by 500 Gy (blue curve) and that of the same exact teeth after the pretreatment of base etching and mechanical crushing (red) (Color figure online)



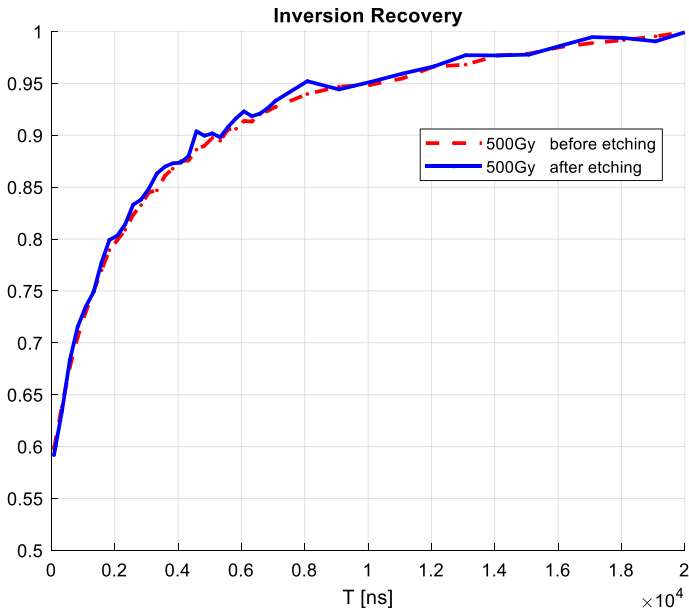


**Fig. 13** Inversion recovery results for the same tooth, irradiated by 500 Gy before and after the pretreatment of base etching and mechanical crushing

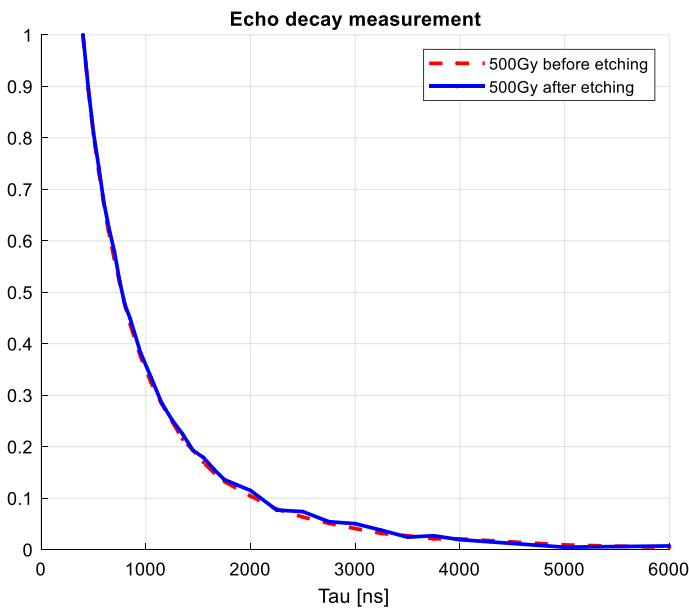


**Fig. 14** Hahn echo decay curve results for the same tooth, irradiated by 500 Gy before and after the pretreatment of base etching and mechanical crushing


**Acknowledgements** This work was partially supported by a grant from Pazy Foundation in Israel

## References

1. M. Port, M. Majewski, M. Abend, Radiation dose is of limited clinical usefulness in persons with acute radiation syndrome. *Radiat. Prot. Dosim.* **186**, 126–129 (2019)
2. H.M. Swartz, B.B. Williams, R.J. Nicolalde, E. Demidenko, A.B. Flood, Overview of biodosimetry for management of unplanned exposures to ionizing radiation. *Radiat Meas* **46**, 742–748 (2011)
3. IAEA, Diagnosis and treatment of radiation injuries. *Saf. Rep. Ser.* **2**, 34–39 (1998)
4. J.E. Moulder, Post-irradiation approaches to treatment of radiation injuries in the context of radiological terrorism and radiation accidents: A review. *Int. J. Radiat. Biol.* **80**, 3–10 (2004)
5. H.M. Swartz, A.B. Flood, R.M. Gougelet, M.E. Rea, R.J. Nicolalde, B.B. Williams, A critical assessment of biodosimetry methods for large-scale incidents. *Health Phys.* **98**, 95–108 (2010)
6. H.M. Swartz, B.B. Williams, B.I. Zaki, A.C. Hartford, L.A. Jarvis, E.Y. Chen, R.J. Comi, M.S. Ernststoff, H.G. Hou, N. Khan, S.G. Swartz, A.B. Flood, P. Kuppusamy, Clinical EPR: Unique opportunities and some challenges. *Acad. Radiol.* **21**, 197–206 (2014)
7. A.B. Flood, H.K. Boyle, G. Du, E. Demidenko, R.J. Nicolalde, B.B. Williams, H.M. Swartz, Advances in a framework to compare bio-dosimetry methods for triage in large-scale radiation events. *Radiat. Prot. Dosim.* **159**, 77–86 (2014). (PMCID4067227)
8. N. Dainiak, J. Albanese, M. Kaushik, A.S. Balajee, A. Romanyukha, T.J. Sharp, W.F. Blakely, Concepts of operations for a US dosimetry and biodosimetry network. *Radiat. Prot. Dosim.* **186**, 130–138 (2019)
9. E.H. Haskell, R.B. Hayes, G.H. Kenner, Improved accuracy of EPR dosimetry using a constant rotation goniometer. *Radiat. Meas.* **27**, 325–329 (1997)
10. IAEA, Use of electron paramagnetic resonance dosimetry with tooth enamel for retrospective dose assessment. *IAEA Publ.* **57**, 1331 (2002)
11. G. Liidja, A. Wieser, Electron paramagnetic resonance of human tooth enamel at high gamma ray doses. *Radiat. Prot. Dosim.* **101**, 503–506 (2002)
12. H. Wolfson, R. Ahmad, Y. Twig, B. Williams, A. Blank, A magnetic resonance probehead for evaluating the level of ionizing radiation absorbed in human teeth. *Health Phys.* **108**, 326–335 (2015)
13. H.M. Swartz, H.G. Hou, N. Khan, L.A. Jarvis, E.Y. Chen, B.B. Williams, P. Kuppusamy, Advances in probes and methods for clinical EPR oximetry. *Oxyg. Transp. Tissue* **812**, 73–79 (2014)
14. H.M. Swartz, A.B. Flood, B.B. Williams, R.H. Dong, S.G. Swartz, X.M. He, O. Grinberg, J. Sidabras, E. Demidenko, J. Gui, D.J. Gladstone, L.A. Jarvis, M.M. Kmiec, K. Kobayashi, P.N. Lesniewski, S.D.P. Marsh, T.P. Matthews, R.J. Nicolalde, P.M. Pennington, T. Reynolds, I. Salikhov, D.E. Wilcox, B.I. Zaki, Electron paramagnetic resonance dosimetry for a large-scale radiation incident. *Health Phys.* **103**, 255–267 (2012)
15. B.B. Williams, R.H. Dong, A.B. Flood, O. Grinberg, M. Kmiec, P.N. Lesniewski, T.P. Matthews, R.J. Nicolalde, T. Reynolds, I.K. Salikhov, H.M. Swartz, A deployable in vivo EPR tooth dosimeter for triage after a radiation event involving large populations. *Radiat. Meas.* **46**, 772–777 (2011)
16. B. Pass, J.E. Aldrich, Dental enamel as an in vivo radiation dosimeter. *Med. Phys.* **12**, 305–307 (1985)
17. R. Grun, H. Kohno, A. Tani, C. Yamanaka, M. Ikeya, H.P. Huang, Pulsed ESR measurements on fossil teeth. *Radiat. Meas.* **27**, 425–431 (1997)
18. M.R. Gafurov, T.B. Biktairov, G.V. Mamin, D.V. Shurtakova, E.S. Klimashina, V.I. Putlyaev, S.B. Orlinskii, Study of the effects of hydroxyapatite nanocrystal codoping by pulsed electron paramagnetic resonance methods. *Phys. Solid State* **58**, 469–474 (2016)
19. M. Marrale, A. Longo, M. Brai, A. Barbon, M. Brustolon, P. Fattibene, Pulsed EPR analysis of tooth enamel samples exposed to UV and gamma-radiations. *Radiat. Meas.* **46**, 789–792 (2011)
20. H. Sato, B.A. Filas, S.S. Eaton, G.R. Eaton, A.A. Romanyukha, R. Hayes, A.M. Rossi, Electron spin relaxation of radicals in irradiated tooth enamel and synthetic hydroxyapatite. *Radiat. Meas.* **42**, 997–1004 (2007)
21. A.D. Milov, A.G. Maryasov, Y.D. Tsvetkov, Pulsed electron double resonance (PELDOR) and its applications in free-radicals research. *Appl. Magn. Reson.* **15**, 107–143 (1998)
22. A. Schweiger, G. Jeschke, *Principles of Pulse Electron Paramagnetic Resonance* (Oxford University Press, Oxford, 2001)

23. S. Stoll, A. Ozarowski, R.D. Britt, A. Angerhofer, Atomic hydrogen as high-precision field standard for high-field EPR. *J. Magn. Reson.* **207**, 158–163 (2010)
24. G. Mitrikas, Pulsed EPR characterization of encapsulated atomic hydrogen in octasilsesquioxane cages. *Phys. Chem. Chem. Phys.* **14**, 3782–3790 (2012)
25. S. Agnello, *Gamma Ray Induced Processes of Pointdefect Conversion in Silica* (Università di Palermo, Palermo, 2000)
26. D.G. Mitchell, R.W. Quine, M. Tseitlin, V. Meyer, S.S. Eaton, G.R. Eaton, Comparison of continuous wave, spin echo, and rapid scan EPR of irradiated fused quartz. *Radiat. Meas.* **46**, 993–996 (2011)
27. G.R. Eaton, S.S. Eaton, R.W. Quine, D. Mitchell, V. Kathirvelu, R.T. Weber, A signal-to-noise standard for pulsed EPR. *J. Magn. Reson.* **205**, 109–113 (2010)
28. A. Blank, Y. Twig, Y. Ishay, Recent trends in high spin sensitivity magnetic resonance. *J. Magn. Reson.* **280**, 20–29 (2017)
29. J.J.L. Morton, A.M. Tyryshkin, A. Ardavan, K. Porfyrakis, S.A. Lyon, G.A.D. Briggs, Measuring errors in single-qubit rotations by pulsed electron paramagnetic resonance. *Phys. Rev. A* **71**, 012332 (2005)
30. S.A. Dzuba, Y.D. Tsvetkov, Magnetization transfer in pulsed EPR of <sup>15</sup>N nitroxides: Reorientational motion model of molecules in glassy liquids. *Chem. Phys.* **120**, 291–298 (1988)
31. B.E. Bode, D. Margraf, J. Plackmeyer, G. Dürner, T.F. Prisner, O. Schiemann, Counting the monomers in nanometer-sized oligomers by pulsed electron–electron double resonance. *J. Am. Chem. Soc.* **129**, 6736–6745 (2007)
32. G.C. Borgia, R.J.S. Brown, P. Fantazzini, Uniform-penalty inversion of multiexponential decay data. *J. Magn. Reson.* **132**, 65–77 (1998)
33. L.M.D. Oliveira, E.D. Jesus, A. Rossi, R. Lopes, L.N. Rodrigues, R. Barbosa, Energy dependence of EPR signal in synthetic and biological hydroxyapatite irradiated with photons. *Radiat. Prot. Dosim.* **84**, 511–514 (1999)
34. D.A. Schauer, M.F. Desrosiers, F.G. Le, S.M. Seltzer, J.M. Links, EPR dosimetry of cortical bone and tooth enamel irradiated with X and gamma rays: Study of energy dependence. *Radiat. Res.* **138**, 1–8 (1994)
35. G.M. Hassan, E. Aboezez, A. El-Khodary, H.M. Eissa, Inter-comparison study between human and cow teeth enamel for low dose measurement using ESR. *Nucl. Instrum. Method B* **268**, 2329–2336 (2010)
36. J.E. Aldrich, B. Pass, Dental enamel as an in vivo radiation dosimeter: Separation of the diagnostic X ray dose from the dose due to natural sources. *Radiat. Prot. Dosim.* **17**, 175–179 (1986)
37. M. Iwasaki, C. Miyazawa, A. Kubota, E. Suzuki, K. Sato, J. Naoi, A. Katoh, K. Niwa, Energy dependence of the CO<sub>33-</sub> signal intensity in ESR dosimetry of human tooth enamel. *Radioisotopes* **40**, 421–424 (1991)
38. J. Tatsumi-Miyajima, ESR dosimetry for atomic bomb survivors and radiologic technologists. *Nucl. Instrum. Methods Phys. Res., Sect. A* **257**, 417–422 (1987)
39. V.A. Serezhnikov, E.V. Domracheva, G.A. Klevezal, S.M. Kulikov, S.A. Kuznetsov, P.I. Mordvintcev, L.I. Sukhovskaya, N.E. Sukhovskaya, A.F. Vanin, N.V. Voevodskaya, A.I. Vorobiev, Radiation dosimetry for residents of the chernobyl region: A comparison of cytogenetic and electron spin resonance methods. *Radiat. Prot. Dosim.* **42**, 33–36 (1992)
40. D.U. Schramm, A.M. Rossi, Electron spin resonance (ESR) studies of CO–2 radicals in irradiated A and B-type carbonate-containing apatites. *Appl. Radiat. Isot.* **52**, 1085–1091 (2000)
41. M. Marrale, M. Brai, A. Barbon, M. Brustolon, Analysis of the spatial distribution of free radicals in ammonium tartrate by pulse epr techniques. *Radiat. Res.* **171**, 349–359 (2009)
42. S.S. Eaton, G.R. Eaton, Irradiated fused-quartz standard sample for time-domain EPR. *J. Magn. Reson. Ser. A* **102**, 354–356 (1993)
43. K.M. Sailkhov, Y.D. Tsvetkov, Electron spin-echo studies of spin-spin interactions in solids, in *Time Domain Electron Spin Resonance*. (John Wiley and Sons, New Jersey, 1979), pp. 231–278
44. A. Brik, E. Haskell, V. Brik, O. Scherbina, O. Atamanenko, Anisotropy effects of EPR signals and mechanisms of mass transfer in tooth enamel and bones. *Appl. Radiat. Isot.* **52**, 1077–1083 (2000)
45. G. Jeschke, G. Panek, A. Godt, A. Bender, H. Paulsen, Data analysis procedures for pulse ELDOR measurements of broad distance distributions. *Appl. Magn. Reson.* **26**, 223–244 (2004)
46. A.D. Milov, A.B. Ponomarev, Y.D. Tsvetkov, Modulation beats of signal of double electron-electron resonance in spin echo for biradical systems. *J. Struct. Chem.* **25**, 710–713 (1984)

## Authors and Affiliations

Lotem Buchbinder<sup>1</sup> · Hanan Datz<sup>2</sup> · Nir Dayan<sup>1</sup> · Raanan Carmieli<sup>3</sup> ·  
Aharon Blank<sup>1</sup> 

✉ Aharon Blank  
ab359@tx.technion.ac.il

<sup>1</sup> Schulich Faculty of Chemistry, Technion–Israel Institute of Technology, Haifa, Israel

<sup>2</sup> Radiation Safety Division, Soreq Nuclear Research Center, Yavne, Israel

<sup>3</sup> Department of Chemical Research Support, Weizmann Institute of Science, Rehovot, Israel